Nanoscale

Cite this: *Nanoscale*, 2012, **4**, 7394

www.rsc.org/nanoscale

PAPER

Diameter and chiral angle distribution dependencies on the carbon precursors in surface-grown single-walled carbon nanotubes†

Maoshuai He,*[a] Hua Jiang,[b] Esko I. Kauppinen[b] and Juha Lehtonen[a]

Received 14th August 2012, Accepted 1st October 2012
DOI: 10.1039/c2nr32276e

Carbon nanotubes grown from discrete Fe-containing nanoparticles dispersed on a silicon nitride transmission electron microscope grid were systematically studied. The (*n*,*m*) indices of produced single-walled carbon nanotubes (SWNTs) were deduced from their electron diffraction patterns. Relatively small diameter SWNTs with a narrow diameter distribution (0.7–1.6 nm) were produced using CO as the carbon source at 800 °C, while large diameter SWNTs ranging from 1.0 nm to 4.7 nm were synthesized when using CH_4 as the carbon source. The chiral angle distributions of the SWNTs produced from different carbon sources are also different, which are attributed to the preferred cap nucleation associated with the carbon feed rate on the catalyst instead of carbon nanotube growth kinetics. Furthermore, growth of carbon laminar nanoclusters inside carbon nanotubes was achieved at a higher growth temperature, suggesting that dissociated carbon diffuses across the nanoparticle during the nanotube growth process.

Introduction

Carbon nanotubes, especially single-walled carbon nanotubes (SWNTs), have been the focus of intensive research due to their extraordinary electrical and optical properties arising from their unique atomic structures.[1] Growing SWNTs with controlled chirality has been one of the most challenging tasks in the carbon nanotube synthesis field.[2–4] In order to achieve this goal, it is necessary to gain more insight into the SWNT formation mechanisms and study the possible factors influencing SWNT chirality. *In situ* techniques such as environmental transmission electron microscopy (TEM)[5,6] and X-ray photoelectron spectroscopy[7] have been applied to investigate the catalyst evolutions and SWNT growth dynamics. However, the understanding of the growth mechanisms and chirality-controlled factors is still incomplete due to the inherent limits in spatial and temporal resolutions furnished by current experimental techniques.

Numerous theoretical studies have been published for complementing the understanding of SWNT nucleation and growth.[8–11] A number of factors, such as catalyst morphology,[8] cap stability,[9] SWNT growth rate[10] and metal–substrate interaction strength,[11] are predicated to affect the final chirality distribution of the SWNTs. A kinetic theory based on the screw dislocation growth mechanisms was proposed by Ding *et al.*,[10] predicting that the dominance of nearly armchair SWNTs is due to their high growth rates proportional to their chiral angles. However, Reich *et al.*[9] proposed that the chirality selective growth of SWNTs could be possibly controlled by caps formed on the catalyst during the nucleation stage. Both models agree with some dispersive experimental results and shed light on the chirality-controlled growth of SWNTs.

The chemistry of the carbon precursor was usually neglected in theoretical work. The dependences of chirality distributions on carbon precursors were studied experimentally for SWNTs grown on some catalysts, such as the CoMo–SiO_2 catalyst.[12,13] Compared with CO, CH_4 usually produces SWNTs with larger diameters and a broad diameter distribution, as evidenced by the absorption and photoluminescence characterization results. Lolli *et al.*[12] attributed the growth of larger diameter SWNTs to the role of H_2, a by-product of CH_4 decomposition. The presence of H_2 delays the formation of SWNT caps and leads to the formation of larger particles by sintering, which results in the production of large diameter SWNTs.[12] However, the failed growth of small diameter SWNTs using CH_4 instead of CO as the carbon source on the porous SiO_2 supported Ni catalyst[14] was also observed at temperatures below 500 °C, at which the sintering process is weakly active. It seems that sintering is not the only factor influencing SWNT chirality when different carbon sources are used. To deeply study the roles of the carbon precursor in determining the final SWNT chiralities, it is necessary to study the chirality distributions of SWNTs grown on a stable catalyst with a reliable characterization technique.

[a]*Department of Biotechnology and Chemical Technology, School of Chemical Technology, Aalto University, P.O. Box 16100, FI-00076 Aalto, Finland. E-mail: maoshuai.he@aalto.fi; Fax: +358 947022622; Tel: +358 947022874*
[b]*Department of Applied Physics and Center for New Materials, School of Science, Aalto University, P.O. Box 15100, FI-00076 Aalto, Finland*

† Electronic supplementary information (ESI) available: Tables of (*n*,*m*) resolved SWNT species grown using CO and CH_4 as carbon sources at 800 °C; TEM images of prepared nanoparticles and carbon nanostructures grown at 950 °C using CH_4 as the carbon precursor. See DOI: 10.1039/c2nr32276e

Different from metal particles dispersed on a porous support, flat substrate supported discrete nanoparticles usually show extreme thermal stability and do not sinter even at high growth temperatures.[15–17] This is mainly due to the embedding of nanoparticles into the substrate.[16] In this work, we will study the SWNTs grown on pre-made Fe particles dispersed onto silicon nitride (Si_3N_4) TEM grids using CO and CH_4 as carbon sources by chemical vapor deposition. In order to gain insight into the possible factors controlling the final SWNT chirality distribution, the diameter and chirality distributions of SWNTs grown using different carbon sources were analyzed and compared. Furthermore, the influences of the growth temperature on the carbon nanotube wall numbers as well as the tube structures were studied, which helps in understanding the carbon diffusion process during growth.

Experimental section

1. Preparation of Fe nanoparticles

The Fe nanoparticles were prepared by chemical reduction of $FeCl_3$ under microwave irradiation.[18] In brief, $FeCl_3$ (0.0008 g) and poly(*N*-vinyl-2-pyrrolidone) (PVP, M_w 40 000, 0.0287 g) were first dissolved in 4.8 mL ethylene glycol. A glycol solution with ammonia (0.02 mL) was added to the $FeCl_3$ solution and the mixture was subsequently irradiated in a microwave oven for 30 s.

2. Growth of carbon nanotubes

The prepared Fe nanoparticles were dispersed onto a Si_3N_4 TEM grid (DuraSiN™ mesh). After drying, the sample was annealed in air at 800 °C to remove the polymers and enhance the interactions between Fe particles and the substrate. The TEM grid was then loaded into a chemical vapor deposition reactor with a quartz tube (inner diameter: 4 cm), which was heated to target temperatures in a flow of Ar (300 cm^3 min^{-1}). CO or CH_4 with a flow rate of 100 cm^3 min^{-1} was then introduced for carbon nanotube growth and the reaction period lasted for 1 h. The reactor was then cooled down under the protection of Ar.

3. Characterization of carbon nanotubes

The carbon nanotubes were investigated using a JEOL-2200FS double aberration-corrected TEM operated at 80 kV. The (*n*,*m*) determination from electron diffraction (ED) patterns of individual SWNTs was based on a calibration-free intrinsic layer line-spacing method.[19,20]

Raman characterization on the carbon nanotubes was performed using a Jobin Yvon LabRam 300 excited with an excitation laser wavelength of 633 nm.

Results and discussions

1. Growth of SWNTs using CO as the carbon precursor

Fig. 1a presents a TEM image of SWNTs grown on the Fe nanoparticles with CO as the carbon precursor at 800 °C, which show that relatively small diameter SWNTs were produced. The production of SWNTs is also verified by the presence of radial breathing modes (RBMs) shown in the Raman spectra (ESI, Fig. S1a†). Extensive TEM characterization did not observe any double-walled or triple-walled carbon nanotubes. ED patterns of randomly distributed individual SWNTs were acquired. Fig. 1b is a representative ED pattern of one individual SWNT, based on which (*n*,*m*) indices of the SWNT can be assigned to (8,4). A total of 93 individual SWNTs were determined by their ED patterns. The results were presented in the ESI, Table S1.† Calculated from the (*n*,*m*) indices, SWNTs with diameters ranging from 0.7 to 1.6 nm and a mean diameter of 1.0 nm were produced under such growth conditions (Fig. 1c). The mean diameter is a bit smaller than that calculated from the RBM frequencies[21] shown in the Raman spectra (1.2 nm, ESI, Fig. S1b†). This is probably because there are less small diameter (<1.0 nm) SWNT species than large diameter ones that are resonant with the 633 nm laser[22]. 28 out of the total 93 SWNTs are metallic ones (30%), *i.e.* preference of either metallic or semiconducting SWNTs was not shown. The chiral angle distribution of the CO-grown SWNTs is presented in Fig. 1d, showing that the chiral angles of SWNTs are not evenly distributed. Despite the existence of zigzag SWNTs with a chiral angle of 0°, such as (12,0) and (14,0), only 8 SWNTs with a chiral angle smaller than 10° were observed (8.6%). There is a strong preference for forming SWNTs with larger chiral angles. 22 (23.7%) SWNTs have chiral angles in the range of 10 to 20°, and more than 66% of SWNTs have chiral angles larger than 20°.

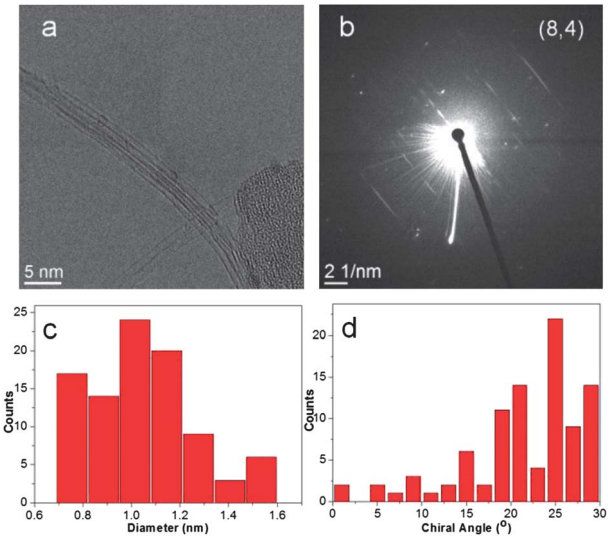

Fig. 1 (a) A TEM image of carbon nanotubes grown on a Si_3N_4 grid supported Fe nanoparticles at 800 °C using CO as the carbon source. (b) ED pattern of one isolated SWNT grown on Fe nanoparticles using CO as the carbon source. (c) The diameter and (d) chiral angle distributions of SWNTs grown at 800 °C using CO as the carbon source.

This observation is somehow in agreement with the growth kinetics controlled chirality distribution based on screw dislocation theory.[10] According to the theory, the SWNT growth rate is proportional to the chiral angle. Consequently, the number of SWNTs is proportional to their respective chiral angles. However, there are some discrepancies. First of all, there are more SWNTs with a chiral angle of approximately 25° instead of SWNTs having a chiral angle of 30°, which are supposed to have the highest growth rate. (8,6) and (9,7) species with respective chiral angles of 25.3° and 25.9° were observed more frequently (8.6% and 9.7%, respectively) than other species (ESI, Table S1†). This observation

is similar to our previous ED characterization results of SWNTs grown on the FeCu–MgO catalyst,[20] where armchair tubes are also not predominant in the product. In addition, the portion of SWNTs (66.7%) with chiral angles larger than 20° is about 10% higher than the portion predicated by the dislocation theory.[10] Such a deviation cannot simply be attributed to the measurement error.

The cap formation energy theory[9,23] should be more applicable in interpreting the SWNT growth result. The SWNT formation starts with the diffusion of carbon on the nanoparticle surface or across its interior, leading to the nucleation of a graphitic fragment. Carbon atoms rearrange readily while they are adsorbed on the catalyst surface to form a favored cap which must be matched locally and globally on a catalyst surface.[9] Once a cap is formed, the carbon nanotube with a unique structure then grows further by the incorporation of carbon. The preferable formation of SWNTs with large chiral angles, as well as some specific species can be ascribed to their relatively low cap formation energies.

2. Growth of SWNTs using CH_4 as the carbon precursor

In order to study the influence of carbon precursors on SWNT chiralities, carbon nanotubes grown on the Fe catalyst using CH_4 were also studied by ED characterizations. As clearly indicated by the RBMs in their Raman spectra, SWNTs were synthesized (ESI, Fig. S2†). Fig. 2a shows a typical TEM image of a carbon nanotube grown at 800 °C. In agreement with SWNTs grown on a porous SiO_2 supported CoMo catalyst using CH_4 as the carbon source,[12,13] the tubes have relatively large diameters compared with CO-grown SWNTs. Fig. 2b presents an ED pattern of a (41,8) SWNT with a diameter of 3.7 nm. Based on the indices of a total of 98 tubes, the diameter distribution of the CH_4-grown SWNTs is obtained. As shown in Fig. 2c, the SWNTs have diameters in the range of 1.0 to 4.7 nm. 85 SWNTs of different structures have been identified and 35 out of 98 SWNTs are metallic ones (ESI, Table S2†). Similarly, there is no preferable growth of SWNTs with a specific conductivity or atomic structure under such growth conditions. However, in contrast to CO grown SWNTs, the chiral angle distribution of the SWNTs does not show a significant preference in the range of 20–30° (Fig. 2d). Such a chirality distribution can be interpreted well by the cap formation energy theory[9] rather than the dislocation theory.[10] Under such growth conditions, it seems that there is no significant energy difference for forming different caps on particles with large diameters.

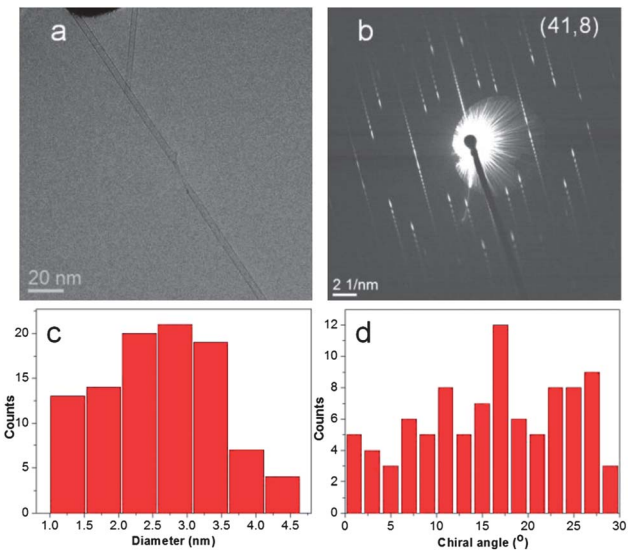

Fig. 2 (a) A TEM image of carbon nanotubes grown on a Si_3N_4 grid supported Fe nanoparticles at 800 °C using CH_4 as the carbon source. (b) The ED pattern of one isolated SWNT grown on Fe nanoparticles using CH_4 as the carbon source. (c) The diameter and (d) chiral angle distributions of SWNTs grown at 800 °C using CH_4 as the carbon source.

What are the reasons for the diverse diameter distribution when different carbon sources are used? It is known that the diameter of a SWNT is correlated with the diameter of the catalyst particle. As shown in the ESI, Fig. S3,† the synthesized Fe nanoparticles have a relatively wide diameter distribution. The formation of large diameter SWNTs from CH_4 is believed to arise from the selective growth of SWNTs on nanoparticles with large diameters. Lu and Liu[24] have demonstrated that the carbon feed rate variation could change the diameter distribution of carbon nanotubes. Under a given carbon feeding rate, only particles with certain diameters are activated and suitable for SWNT growth. Nanoparticles smaller than the optimal value are overfed and tend to form the graphite shell preventing SWNT nucleation, while larger diameter particles cannot be activated due to the underfeeding.[24] CO disproportionate catalytically on the surface of the iron particles by the Boudouard reaction: $CO + CO \rightarrow CO_2 + C$ (s), leading to the nucleation and growth of SWNTs. At a given temperature and pressure, the CO disproportionation is much slower than thermal decomposition of CH_4.[25] The carbon feed rate in the case of CO is thus much slower and only nanoparticles smaller than 1.6 nm are activated for growing SWNTs. When CH_4 is used as the carbon source, small diameter nanoparticles (<1 nm) are poisoned due to overfeeding of carbon resulting from much higher carbon rate. Consequently, only large diameter particles catalyze the nucleation and growth of SWNTs.

H_2, the byproduct of thermal decomposition of CH_4, also plays important roles in nucleating SWNTs with large diameters. It has been proposed that H_2 can decrease the fugacity of carbon on the metal surface of the CoMo–SiO_2 catalyst and thus delay the nucleation of carbon cap.[12] This delay results in the relatively low concentration of small diameter SWNTs when CH_4 is used as the carbon source. On the other hand, hydrogen has a negative blocking effect on the formation of small diameter SWNTs,[26] which have a high tube curvature and a strong tendency for the equilibrium carbon atom to form sp^3 hybridization.[27] In the SWNT growth process, the hydrogen is supposed to destroy the formed caps guiding the growth of small diameter SWNTs at the nucleation stage. To further confirm the roles of H_2, we introduced a mixture of CO and H_2 (1 : 4) as the carbon feed for growing carbon nanotubes. No tubes were observed growing due to the excessive amount of H_2.

3. High temperature growth of carbon nanotubes

In order to study the effects of growth temperature and to gain more insight into the carbon nanotube growth mechanisms, carbon nanotubes were grown at a temperature of 950 °C using

CH_4 as the carbon source. Large diameter carbon nanotubes were produced owing to the fast carbon feed rate.[24] Besides SWNTs, double-walled and a small number of triple-walled carbon nanotubes were also observed. The wall number distribution of the produced carbon nanotubes is shown in Fig. S4 (ESI†). From the close view of the tubes (Fig. 3a and b), it can be seen that carbon laminar nanoclusters[28] formed inside carbon nanotubes. The filling of the carbon laminar nanoclusters inside the tubes was confirmed by heat treatment in a high vacuum (10^{-6} mbar) at 1000 °C. Fig. 3c presents the TEM image of the nanostructure after high vacuum calcinations. No damage was made to the carbon nanotube walls owing to the relatively low temperature applied here.[28] The outer surface of the tube was clean and the carbon laminar nanoclusters remained inside owing to the encapsulation by the closed-end tube. In addition, by tilting structure along the tube axis in TEM, we further confirm that the carbon laminar nanoclusters appear inside the nanotube (ESI, Fig. S5†).

It has been argued whether the carbon is transported to the carbon nanotube open ends through a bulk diffusion process or only by a surface diffusion. The absence of metal carbide that originated from the penetration of carbon into metal particles was observed in Ni catalyzed growth of SWNTs by *in situ* environmental TEM investigations.[6,29] Recent quantum chemical molecular dynamics simulations also demonstrate that the formation of metal carbide is not necessary for metal-catalyzed SWNT nucleation.[30] However, formation of a fluctuating Fe_3C carbide structure was reported by Yoshida *et al.*[5] when growing carbon nanotubes on Fe particles. The contradictory findings appear to be system-dependent.

In our system, the formation of carbon laminar nanoclusters with a certain length inside the carbon nanotube provides a clear evidence for the penetration of carbon into the Fe nanoparticles during the growth process. One of the fundamental roles of the catalyst particle is to prevent the closure of the formed sp^2-hybridized carbon cap by the formation of carbon–metal bonds at the open ends.[31] Carbon atoms by surface diffusion can only be added to the chemically active carbon nanotube edges or form nanoclusters attached to the outer surfaces of the tube. To form such a carbon structure as shown in Fig. 3, bulk diffusion of carbon through the catalyst particle is necessary: (1) Fe catalyst particles are first reduced with the introduction of CH_4; (2) carbon dissolute into the reduced Fe particles; (3) dissolved carbon segregates to form carbon rings and chains on the surface; (4) formation of the carbon cap by merging of carbon structures and subsequent cap lift-off;[11] (5) continuous dissolution and segregation of carbon leads to the new cap formation and tube lengthening; (6) particle morphology evolution[32] of the catalyst particle driven by the carbon cap lift-off favors the formation of disordered carbon laminar nanoclusters instead of a new cap inside the already formed tube; (7) continued growth of carbon nanotubes and carbon laminar nanoclusters (Fig. 3d). In general, the formation of carbon nanoclusters inside the carbon nanotube is related to the excessive decomposition of CH_4 at such a high temperature. The catalytic particles are oversaturated by carbon atoms, precipitating on the surface of nanoparticles and forming the carbon nanoclusters. In order to obtain substantially better understanding to the novel carbon nanostructure growth mechanisms, further experimental and/or calculation work is required.

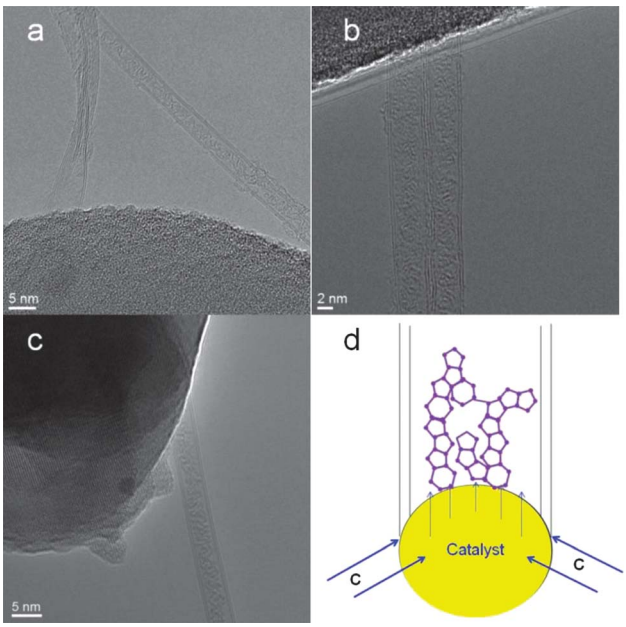

Fig. 3 (a and b) TEM images of carbon nanostructures grown at 950 °C using CH_4 as the carbon source. (c) A TEM image of the carbon nanostructures after being calcined in a high vacuum at 1000 °C for 20 h. (d) The schematic illustration of carbon laminar nanoclusters formation through the bulk diffusion of carbon.

Conclusions

In conclusion, SWNTs were grown on Fe-containing catalysts using CO and CH_4 as carbon precursors, respectively. Both diameter and chiral angle distributions of SWNTs in two samples were quite different, which can be attributed to the preferable cap formation mechanisms and different carbon feed rates. Meanwhile, the killing of caps for nucleating small diameter SWNTs by H_2 is another cause of producing relatively large diameter growth when CH_4 is used. Finally, a novel carbon nanotube-based structure was synthesized, providing clear evidence for the bulk diffusion of carbon through nanoparticles during the carbon nanotube growth process. All the findings here help in understanding the mechanisms of carbon nanotube growth and controlling the diameter and even chirality of SWNTs by fine-tuning the growth parameters.

Notes and references

1 R. H. Baughman, A. A. Zakhidov and W. A. de Heer, *Science*, 2002, **297**, 787–792.
2 W. H. Chiang and R. Mohan Sankaran, *Nat. Mater.*, 2009, **8**, 882–886.
3 S. M. Bachilo, L. Balzano, J. E. Herrera, F. Pompeo, D. E. Resasco and R. B. Weisman, *J. Am. Chem. Soc.*, 2003, **125**, 11186–11187.
4 M. He, A. I. Chernov, P. V. Fedotov, E. D. Obraztsova, J. Sainio, E. Rikkinen, H. Jiang, Z. Zhu, Y. Tian, E. I. Kauppinen, M. Niemela and A. O. Krause, *J. Am. Chem. Soc.*, 2010, **132**, 13994–13996.
5 H. Yoshida, S. Takeda, T. Uchiyama, H. Kohno and Y. Homma, *Nano Lett.*, 2008, **8**, 2082–2086.
6 S. Hofmann, R. Sharma, C. Ducati, G. Du, C. Mattevi, C. Cepek, M. Cantoro, S. Pisana, A. Parvez, F. Cervantes-Sodi, A. C. Ferrari, R. Dunin-Borkowski, S. Lizzit, L. Petaccia, A. Goldoni and J. Robertson, *Nano Lett.*, 2007, **7**, 602–608.

7 S. A. Steiner, 3rd, T. F. Baumann, B. C. Bayer, R. Blume, M. A. Worsley, W. J. MoberlyChan, E. L. Shaw, R. Schlogl, A. J. Hart, S. Hofmann and B. L. Wardle, *J. Am. Chem. Soc.*, 2009, **131**, 12144–12154.
8 P. B. Balbuena, J. Zhao, S. Huang, Y. Wang, N. Sakulchaicharoen and D. E. Resasco, *J. Nanosci. Nanotechnol.*, 2006, **6**, 1247–1258.
9 S. Reich, L. Li and J. Robertson, *Chem. Phys. Lett.*, 2006, **421**, 469–472.
10 F. Ding, A. R. Harutyunyan and B. I. Yakobson, *Proc. Natl. Acad. Sci. U. S. A.*, 2009, **106**, 2506–2509.
11 D. A. Gomez-Gualdron, G. D. McKenzie, J. F. Alvarado and P. B. Balbuena, *ACS Nano*, 2012, **6**, 720–735.
12 G. Lolli, L. Zhang, L. Balzano, N. Sakulchaicharoen, Y. Tan and D. E. Resasco, *J. Phys. Chem. B*, 2006, **110**, 2108–2115.
13 B. Wang, C. H. P. Poa, L. Wei, L.-J. Li, Y. Yang and Y. Chen, *J. Am. Chem. Soc.*, 2007, **129**, 9014–9019.
14 M. He, A. I. Chernov, E. D. Obraztsova, J. Sainio, E. Rikkinen, H. Jiang, Z. Zhu, A. Kaskela, A. G. Nasibulin, E. I. Kauppinen, M. Niemelä and O. Krause, *Nano Res.*, 2011, **4**, 334–342.
15 G.-H. Jeong, S. Suzuki, Y. Kobayashi, A. Yamazaki, H. Yoshimura and Y. Homma, *Appl. Phys. Lett.*, 2007, **90**, 043108.
16 G.-H. Jeong, A. Yamazaki, S. Suzuki, Y. Kobayashi and Y. Homma, *Chem. Phys. Lett.*, 2006, **422**, 83–88.
17 M. He, X. Duan, X. Wang, J. Zhang, Z. Liu and C. Robinson, *J. Phys. Chem. B*, 2004, **108**, 12665–12668.
18 X. Wang, W. Yue, M. He, M. Liu, J. Zhang and Z. Liu, *Chem. Mater.*, 2004, **16**, 798–805.
19 H. Jiang, A. Nasibulin, D. Brown and E. Kauppinen, *Carbon*, 2007, **45**, 662–667.
20 M. He, B. Liu, A. I. Chernov, E. D. Obraztsova, I. Kauppi, H. Jiang, I. Anoshkin, F. Cavalca, T. W. Hansen, J. B. Wagner, A. G. Nasibulin, E. I. Kauppinen, J. Linnekoski, M. Niemelä and J. Lehtonen, *Chem. Mater.*, 2012, **24**, 1796–1801.
21 A. Jorio, R. Saito, J. Hafner, C. Lieber, M. Hunter, T. McClure, G. Dresselhaus and M. Dresselhaus, *Phys. Rev. Lett.*, 2001, **86**, 1118–1121.
22 R. B. Weisman and S. M. Bachilo, *Nano Lett.*, 2003, **3**, 1235–1238.
23 S. Reich, L. Li and J. Robertson, *Phys. Rev. B: Condens. Matter Mater. Phys.*, 2005, **72**, 165423.
24 C. Lu and J. Liu, *J. Phys. Chem. B*, 2006, **110**, 20254–20257.
25 P. Nikolaev, M. J. Bronikowski, R. K. Bradley, F. Rohmund, D. T. Colbert, K. A. Smith and R. E. Smalley, *Chem. Phys. Lett.*, 1999, **313**, 91–97.
26 G. Zhang, *Proc. Natl. Acad. Sci. U. S. A.*, 2005, **102**, 16141–16145.
27 S. Park, D. Srivastava and K. Cho, *Nano Lett.*, 2003, **3**, 1273–1277.
28 Y. A. Kim, H. Muramatsu, T. Hayashi, M. Endo, M. Terrones and M. S. Dresselhaus, *Chem. Phys. Lett.*, 2004, **398**, 87–92.
29 M. Lin, J. P. Ying Tan, C. Boothroyd, K. P. Loh, E. S. Tok and Y. L. Foo, *Nano Lett.*, 2006, **6**, 449–452.
30 Y. Ohta, Y. Okamoto, A. J. Page, S. Irle and K. Morokuma, *ACS Nano*, 2009, **3**, 3413–3420.
31 A. Thess, R. Lee, P. Nikolaev, H. Dai, P. Petit, J. Robert, C. Xu, Y. H. Lee, S. G. Kim, A. G. Rinzler, D. T. Colbert, G. E. Scuseria, D. Tomanek, J. E. Fischer and R. E. Smalley, *Science*, 1996, **273**, 483–487.
32 E. Pigos, E. S. Penev, M. A. Ribas, R. Sharma, B. I. Yakobson and A. R. Harutyunyan, *ACS Nano*, 2011, **5**, 10096–10101.

